



Multivariate optimization of characteristic parameters of continuous-flow system with a front buffer tank for industrial reverse osmosis concentrate treatment

Shida Li^a, Fantang Zeng^{a,*}, Shaokui Zheng^b, Zhongya Fan^a, Lu Huang^a

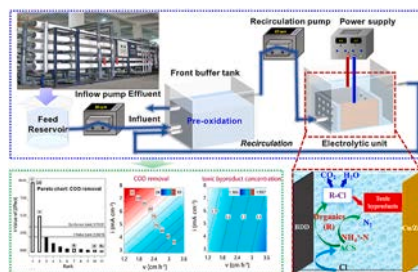
^a The Key Laboratory of Water and Air Pollution Control of Guangdong Province, South China Institute of Environmental Sciences, Ministry of Ecology and Environment, No. 18 Ruihe Road, Guangzhou, 510530, China

^b School of Environment, MOE Key Laboratory of Water and Sediment Sciences/State Key Lab of Water Environment Simulation, Beijing Normal University, Beijing, 100875, China

HIGHLIGHTS

- R , ν values and current density significantly influenced the performance of CFS-C system.
- R_V value and electrode gap can be further optimized to reduce the fixed investment.
- The CCD-RSM models were more efficient than PBD models in predicting the responses.
- Multivariate coordination can optimize the parameters of industrial ROC treatment process.
- High inflow load of CFS-C system should be set according to COD removal CCD-RSM model.

GRAPHICAL ABSTRACT



ARTICLE INFO

Handling Editor: Dr. E. Brillas

Keywords:

Industrial reverse osmosis concentrate
Electrochemical treatment
High effluent quality
Multivariate optimization
Toxic byproduct control

ABSTRACT

Industrial reverse osmosis concentrate (ROC) was electrochemically oxidized using a continuous-flow system (CFS) with a front buffer tank. Multivariate optimization including Plackett-Burman (PBD) and central composite design based on response surface method (CCD-RSM) was implemented to investigate the effects of characteristic (e.g., recirculation ratio (R value), ratio of buffer tank and electrolytic zone (R_V value)) and routine (e.g., current density (i), inflow linear velocity (ν) and electrode spacing (d)) parameters. R , ν values and current density significantly influenced chemical oxygen demand (COD) and NH_4^+-N removal and effluent active chlorine species (ACS) level, while electrode spacing and R_V value had negligible effects. High chloride content of industrial ROC facilitated the generation of ACS and subsequent mass transfer, low hydraulic retention time (HRT) of electrolytic cell improved the mass transfer efficiency, and high HRT of buffer tank prolonged the reaction between the pollutants and oxidants. The significance levels of COD removal, energy efficiency, effluent ACS level and toxic byproduct level CCD-RSM models were validated by statistical test results, including higher F value than critical effect value, lower P value than 0.05, low deviation between predicted and observed values, and normal distribution of calculated residuals. The highest pollutant removal was achieved at a high R value, a high current density and a low ν value; the highest energy efficiency was achieved at a high R , a low current

* Corresponding author.

E-mail address: zengfantang@scies.org (F. Zeng).

<https://doi.org/10.1016/j.chemosphere.2023.139078>

Received 19 March 2023; Received in revised form 20 May 2023; Accepted 28 May 2023

Available online 31 May 2023

0045-6535/© 2023 Elsevier Ltd. All rights reserved.

density and a high v value; the lowest effluent ACS and toxic byproduct levels were achieved at a low R value, a low current density and a high v value. Following the multivariate optimization, the optimum parameters were decided to be $v = 1.2 \text{ cm h}^{-1}$, $i \geq 8 \text{ mA cm}^{-2}$, $d \geq 4$, $R_V = 10\text{--}20$ and $R = 1$ to achieve better effluent quality (i.e., lower effluent pollutant, ACS and toxic byproduct levels).

Credit author statement

Shida Li: Conceptualization, Investigation, Methodology, Software, Validation, Data curation, Writing–original draft, Writing–review & editing, Visualization, **Fantang Zeng:** Conceptualization, Writing–review & editing, Supervision, **Shaokui Zheng:** Conceptualization, Writing–review & editing, Project administration, Funding acquisition, **Zhongya Fan:** Methodology, Supervision, **Lu Huang:** Methodology, Data curation, Visualization.

1. Introduction

While the coal chemical industry serves as an important feedstock for many industrial sectors, abundant wastewater with complex compositions (e.g., polycyclic aromatic hydrocarbons and nitrogenous heterocyclic compounds (Li et al., 2021) and total dissolved solids (Shi et al., 2020)) is generated during the production process. A combined process including pretreatment, biochemical treatment, and reuse treatment is usually implemented to achieve zero liquid discharge (ZDL) of coal chemical wastewater. Currently, a typical reuse technology, i.e., reverse osmosis (RO) technology, has been widely applied in coal chemical factory due to its capacity for producing reclaimed water with high quality (Lan et al., 2018; Liu et al., 2019b). However, a considerable amount of water is converted into a waste stream (i.e., RO concentrate (ROC)), which often contains high levels of toxic refractory organics and nutrient substances and has high salinity (Lan et al., 2018; Li et al., 2022). In most engineering practices, various evaporation-crystallization processes (e.g., multi-stage flash evaporation (Ihm et al., 2016) or spray dryer (Panagopoulos et al., 2019)) were used to achieve ZDL treatment of ROC to reduce the environmental risks. Some membrane technologies (e.g., forward osmosis, membrane distillation or electrodialysis (Panagopoulos et al., 2019)) were used to pre-concentrate ROC to reduce the operational costs. However, a certain amount of recalcitrant organics could cause severe microbial membrane pollution (Tijing et al., 2015) and disturb the operation of the evaporator and crystallizer (Li et al., 2021).

Electrochemical technology offers advantages for ROC pretreatment including effective and robust control of reaction conditions, in-situ generation of oxidants and operation at ambient temperature and pressure (Bagastyo et al., 2011; Radjenovic et al., 2011), thus having great potential to support the stable operation of ZDL treatment process. However, high energy requirements (Soriano et al., 2019), high residual ACS levels in effluent (Ndlwana et al., 2020), and remarkable formation trends of toxic byproducts (Bagastyo et al., 2011) have considerably limited the wide application of electrochemical technology. Currently, most studies were solely devoted to the optimization of electrolytic parameters for batch systems, while a few studies have investigated the potential effects of specific parameters (Kaur et al., 2018a, 2019; Le et al., 2019) on the performance of continuous-flow system (CFS). An overall survey identified three continuous-flow electrolytic system (CFS) types those had been widely-used, including CFS without electrolytic effluent recirculation (Kaur et al., 2018a) (i.e., CFS-A system), CFS system with a rear buffer tank (Radjenovic et al., 2011) (i.e., CFS-B system) and CFS system with a front buffer tank (Dominguez-Ramos and Irabien, 2013) (i.e., CFS-C system), whereas only few studies have optimized the parameters of the CFS system with recirculation (Radjenovic et al., 2011; Basha et al., 2012). Our previous study has demonstrated that the introduction of effluent recirculation in the CFS-B and –C system increases energy efficiency by 2.1–2.4-fold and decreases

effluent COD level by 3.8–5.4-fold compared with the CFS-A system, attributed to the reutilization of long-lived active ACS oxidants. Moreover, a lower actual inflow rate of the electrochemical cell and significant consumption of ACS oxidants by oxygen-consuming substances entered into the front buffer tank of the CFS-C system considerably reduce the effluent ACS level by 60% compared with CFS-B system (Li et al., 2022). Finally, the CFS-C system is finally recommended for future engineering implementation.

The existences of effluent recirculation and buffer tank are identified as important characteristics of the CFS system with recirculation. An overall survey showed a considerable range of the correlative parameter levels, i.e., recirculation ratio (R) and ratio of buffer tank and electrolytic zone (R_V) which had been set in previous studies as 12 and 1 (Radjenovic et al., 2011) of the CFS-B system, and 27–133 (Basha et al., 2012; Dominguez-Ramos and Irabien, 2013) and 4.2 (Basha et al., 2012) (or ~286 (Dominguez-Ramos and Irabien, 2013)) of the CFS-C system respectively. The significant differences of R and R_V values not only influenced the investments and operative costs, but also the pollutant removal performance of the electrolytic system. Unfortunately, the potential effects of R and R_V values have not received much attention so far for the treatment of wastewater. Moreover, there have been no systematic investigations concerning the potential effects of individual effects and interactions between the characteristic (i.e., R and R_V values) and routine (i.e., inflow linear velocity, v value), current density and electrode spacing) parameters on energy consumption, pollutant removal, as well as effluent ACS and toxic byproduct levels.

In this study, we first adopted Plackett-Burman design (PBD) to screen the significant variables and investigate the potential effects of significant variables on the performance of CFS-C system; the first order polynomial models were optimized. Subsequently, we adopted central composite design based on response surface method (CCD-RSM) to investigate the individual effects and interactions of statistically significant variables; the CCD-RSM polynomial models were also optimized. Finally, we adopted the multivariate optimization tool using with desirability function to simultaneously optimize the parameters of the CFS-C system.

2. Materials and methods

2.1. ROC, electrolytic system and analytical method

The ROC used in this study (189 mg L^{-1} COD, $2.6 \text{ mg L}^{-1} \text{ NH}_4^+ \text{ -N}$, 32 mS cm^{-1} conductivity, $4549 \text{ mg L}^{-1} \text{ Cl}^-$) was collected from the secondary RO unit of a full-scale coal chemical wastewater treatment plant (Shenhua Ningxia Coal Chemical Co. Ltd, Ningdong City, Ningxia Province, China). Electrolytic experiments were performed in a CFS-C system (Fig. 1), including a plexiglass single-compartment electrochemical cell placed horizontally (established by Li et al. (2022)), a precision-regulated power supply (PS-305D, ZHAOXIN, Shanghai, China), a 3-L feed tank, a buffer tank, two peristaltic pumps (BT100-2J, LongerPump, Baoding, China). The details of the electrolytic system and analytical methods are provided in Supplementary Text S1.

2.2. Screening of significant variables and optimization of first-order models by means of PBD

In this work, we adopted PBD for screening and identifying the variables those significantly influenced the performance of the CFS-C system. The statistical software package Design Expert (v.20, Stat-Ease

Inc., Minneapolis, USA) was used for conducting the analysis. Of the 11 variables screened, 5 comprised of actual variables (i.e., R , R_V and ν values, current density and electrode spacing) and the remaining six were dummy variables. Each variable was set at two levels (Table S1), i.e., high (+1) and low (-1), where the high/low levels were decided based on literature and our previous study (Supplementary Text S2). Center point (0) was defined as the average of the high and low settings. Out of the matrix of 15 runs, 3 were replicates of the center point and the remaining 12 were composed of various combinations of the 11 factors, as shown in Table S2. One-way analysis of variance (ANOVA), diagram of relationship between predicted and measured values, and pareto chart of effects were used to identify the significance levels of the PBD polynomial models, determine the significant variables and optimize the models.

2.3. Optimization of CCD-RSM polynomial models and electrolytic conditions

A three-factor CCD-RSM was then conducted to investigate the potential effects of significant variables on the pollutant removal, energy efficiency, effluent ACS and toxic byproduct levels, and to simultaneously optimize the levels of the significant variables. The levels of significant variables were established in accordance with the geometry of the design and the ranges previously used in the PBD. The analysis of the experimental data was supported by Design Expert, including ANOVA, diagram of relationship between predicted and measured values, and normal probability plot of residuals to identify the significance levels of the CCD-RSM models. Then the contour diagrams were used to investigate the individual effects and interactions of various variables, and to determine the optimum conditions for each response achieving the optimum level. Finally, the simultaneous optimization of variables was performed using the multivariate optimization tool with desirability function. All the experiments in the PBD and CCD-RSM were performed randomly to minimize the effect of uncontrolled factor that may introduce bias.

3. Results and discussion

Besides the electrolytic system type, operational conditions could impact the performance of electrolytic system, it is of great practical significance to carry out the research for optimization of operational parameters with specific electrolytic performance for ROC treatment. In this study, the multivariate optimization process was performed using the RSM strategy. The PBD was used to study the effects of five parameters such as R , R_V and ν values, current density and electrode spacing on COD, NH_4^+-N removal and effluent ACS level, while the CCD-RSM was used to further study the effects of significant parameters such as R , ν values and current density on pollutant removal, energy efficiency, effluent ACS and toxic byproduct levels.

3.1. Screening of significant variables and optimization of first-order models by means of PBD

A PBD is widely used (e.g., electrochemical sensor synthesis (Armas et al., 2016; Nezhadali and Mojarab, 2016) and polymer material synthesis (Ding et al., 2020)) to screen significant variables. The obtained model from PBD, i.e., first-order polynomial model, does not describe the interaction between the parameters (Nezhadali and Mojarab, 2016). The analysis process of the PBD experiment data was described as follows: (1) The multivariate regression analysis was performed to obtain the first-order polynomial models (Eq. (S1)–(S3) in Supplementary Text S2); (2) The quality of polynomial models was evaluated by exploiting ANOVA (including R^2 and R_{adj}^2 values, adequate precision, F test absolute value of effect (i.e., $|E_{\text{crit}}|$ or F value) and $\text{prob} > F$ value (i.e., P value), Table 1), predicted-observed plots (Fig. 2) and residual-predicted plots (Fig. S6); (3) The significance of each variable was validated by exploiting ANOVA (including F and P values, and % contribution, Table 1) and pareto charts (Fig. 3), and the optimized polynomial models (Eqs. (1)–(3)) were subsequently obtained by

Table 1

Analysis of statistical significance levels of the polynomial models and variables included in the PBD.

Source	Sum of Squares	df	Mean Square	F-value	P-value	% contribution
P_{R-COD} (%)						
Model ^a	4716	5	943	27	<0.0001*	
R	10	1	10	0.29	0.60	0.20
ν	990	1	990	29	0.0007*	20
i	3710	1	3710	108	<0.0001*	74
a	4.1	1	4.1	0.12	0.74	0.08
R_V	2.1	1	2.1	0.06	0.81	0.04
Residual	275	8	34			
P_{R-NH₄⁺-N} (%)						
Model ^b	17589	5	3518	92	<0.0001*	
R	44	1	44	1.2	0.31	0.20
ν	0.75	1	0.75	0.02	0.89	0.0004
i	17404	1	17404	455	<0.0001*	81
a	0.08	1	0.08	0.002	0.96	0.003
R_V	140	1	140	3.7	0.09*	0.65
Residual	306	8	38			
P_A (mg L⁻¹)						
Model ^c	173000	5	34528	16	0.0006*	
R	25866	1	25866	12	0.01*	13
ν	3668	1	3668	1.65	0.23	1.9
i	138600	1	138600	62	<0.0001*	72
a	1853	1	1853	0.83	0.38	0.97
R_V	2629	1	2629	1.2	0.31	1.4
Residual	17781	8	2223			

*Statistically significant at $\alpha = 0.05$.

^a $R^2 = 0.94$; $R_{\text{adj}}^2 = 0.91$; adequate precision = 14.

^b $R^2 = 0.98$; $R_{\text{adj}}^2 = 0.97$; adequate precision = 21.

^c $R^2 = 0.91$; $R_{\text{adj}}^2 = 0.85$; adequate precision = 12.

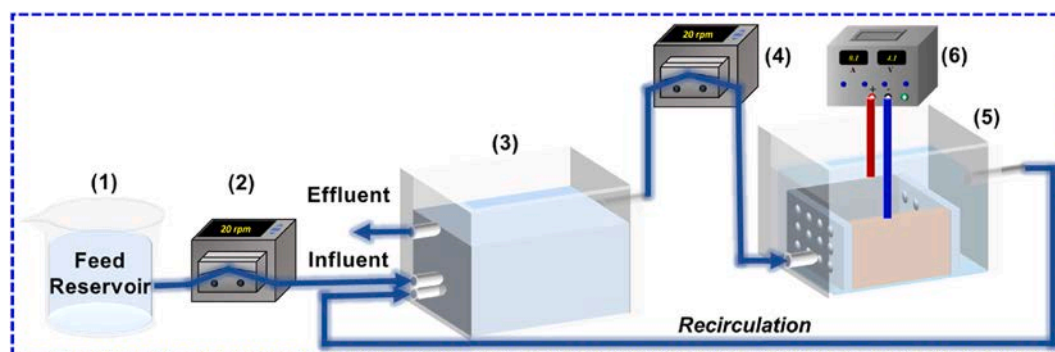


Fig. 1. The CFS-C system: (1) feed tank; (2, 4) pump; (3) buffer tank; (5) electrochemical unit; and (6) power supply.

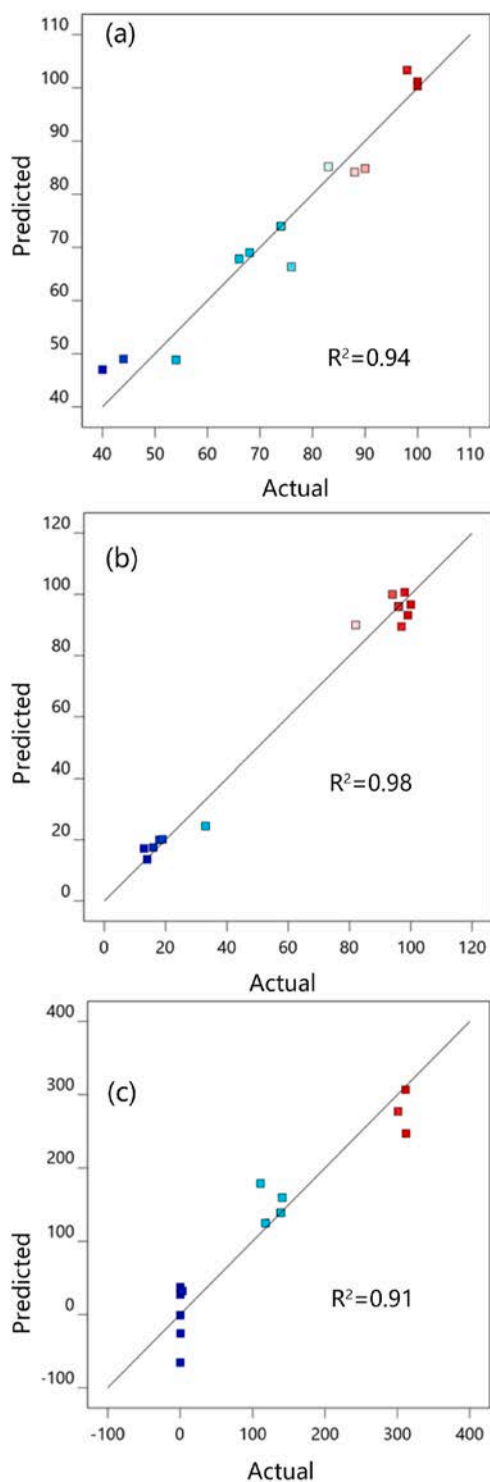


Fig. 2. Predicted versus actual values in the PBD: (a) COD removal, (b) NH_4^+-N removal and (c) effluent ACS level.

removing statistically insignificant variables.

Figs. S1 and S2 show the fluctuating variations of effluent COD, NH_4^+-N , and ACS levels (Fig. S1) and pH, water temperature and conductivity levels and voltages (Fig. S2) in the PBD experiments. The fluctuating variations of physicochemical indexes within narrow ranges indicated the CFS-C system remained under a quasi-steady state. Table S2 shows the experimental domain of the variables and summarizes the mean values and standard deviations of all responses. The first-order regression models are shown as Eqs. (S1)–(S3) in Supplementary

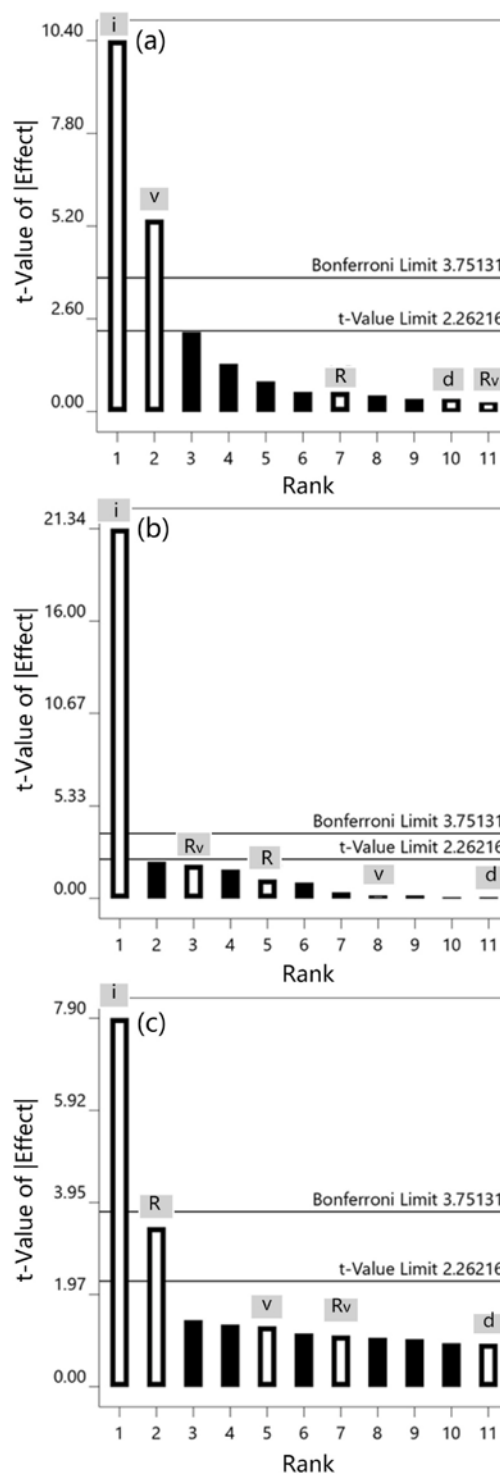


Fig. 3. Pareto chart of t-value of |effect| in the PBD: (a) COD removal, (b) NH_4^+-N removal and (c) effluent ACS level.

Text S2. ANOVA is always used to investigate the significance levels of polynomial models and independent variables (Nezhadali and Mojarab, 2016; Ghosh and Mukherji, 2018). A detailed description of ANOVA is included as Supplementary Text S3. The E_{crit} value obtained applying the modified algorithm of Dong approach (Armas et al., 2016) was 2.26. Validation of the statistical results is analyzed using ANOVA presented in Table 1, in the terms of R^2 and R_{adj}^2 values, adequate precision, F and P values and % contribution. Figs. 2–3 and S6 display the predicted-observed plots (Fig. 2), Pareto charts (Fig. 3) and

residual-predicted plots (Fig. S6). The responses were well fitted to the polynomial models with high R^2 , R_{adj}^2 and adequate precision (Table 1). A F-value higher than E_{crit} and P-value less than 0.05 in the ANOVA indicate the statistical significance of a polynomial model or variable at the 95% confidence level (Thakur et al., 2009; Armas et al., 2016; Ghanbari et al., 2017), while a P value higher than 0.1 indicates a model or variable is insignificant (Cruz-González et al., 2010; Kaur et al., 2018a). In this study, the PBD model F and P values showed that the models estimated by the regression procedure were significant at the 95% confidence level. Additionally, the excellent linear regression fits between predicted and observed values (Fig. 2), as well as randomness of residual distribution (Fig. S6), indicated that all models were perspective in studying the effects of influencing factors on the responses. Of five variables studied, v , R and i had considerable influences at the 95% confidence level. With regards to the COD removal model, the P values of estimated coefficients of v and i were significantly less than 0.05, indicating they were significantly related to the response COD removal. The Pareto chart of effects (Fig. 3a) revealed that the $|E_{crit}|$ values of effects for i and v overpassed t-value limit, implying that they exerted statistically significant influences. Meanwhile, the $|E_{crit}|$ values of effects for R_V , R and electrode spacing were lower than the significance line, which can be attributed to random statistical errors (Chatzisyneon et al., 2009; Zhang et al., 2010) or the factors can be regarded as insignificant variables (Domínguez et al., 2010; Velegraki et al., 2010). The % contribution of i and v was 74 and 20%, respectively, whereas the total % contribution of other three variables was only 0.32%. As for the NH_4^+-N removal model, only i was statistically significant, while other variables exerted statistically insignificant influences (Table 1 and Fig. 3b). As for the ACS level model, the roles of R and i were more important than those of R_V and electrode spacing (Table 1 and Fig. 3c).

There are studies established that a small electrode spacing improves the pollutant removal (Jin et al., 2014), decreases the resistance and energy consumption (Liu et al., 2019a) (due to the resistance depends almost linearly on the electrode spacing (Martinez-Huitle et al., 2015)), while other ones report the opposite trend observing the decrease of current efficiency and increase of electrode maintenance complexity when a small electrode spacing is adopted (Jin et al., 2014). In this study, although the electrode spacing had a negligible effect on the performance of the CFS-C system, the increase of electrode spacing could lead to the reduction of mass transfer resistance of pollutants and oxidants. This is because the gas generation rate and thickness of gas bubble layer decreases as the electrode spacing increases (Liu et al., 2018). Moreover, the greater electrode spacing had the potential for reducing the fixed investment. The front buffer tank could be regarded as one advanced oxidation reactor, thus oxygen-consuming substances entered into the buffer tank could be removed by ACS oxidants generated in the electrochemical cell. Under these conditions, the HRT of buffer tank (5.6–33 h) was significantly greater than that of the previous advanced system (e.g., ~1.3 h of ozone-biological activated carbon system (Lee et al., 2009)), leading to the prolonged reaction between the pollutants and oxidants. Therefore, the performance of the CFS-C system under the conditions of smaller R_V value and greater electrode spacing need to be further optimized to reduce the fixed investment. After removing the coefficients having negligible influences, the optimized polynomial models of COD, NH_4^+-N removal and ACS level (i.e., P_{R-COD} (opt.), $P_{R-NH_4^+-N}$ (opt.) and $P_{A(opt.)}$) are found to be:

$$P_{R-COD(opt.)} = 76.63 - 7.57v + 3.90i \quad (1)$$

$$P_{R-NH_4^+-N(opt.)} = 17.50 + 8.46i \quad (2)$$

$$P_{A(opt.)} = -50.65 + 23.21R + 23.39v \quad (3)$$

3.2. Optimization of CCD-RSM polynomial models

A CCD-RSM is applied in the optimization of variables which are considered significant according to the results obtained in the PBD. During the optimization process of the CCD-RSM, relationship of response, main variables, and interactions can be formulated as a quadratic model (Nezhadali and Mojarrab, 2016). The analysis process of CCD-RSM experiment data was described as follows: (1) The multi-variate regression analysis was performed to obtain the polynomial models of pollutant removal, energy efficiency, effluent ACS and toxic byproduct levels (Eq. (S13)–(S16) in Supplementary Text S4); (2) The quality of polynomial models was evaluated by exploiting ANOVA (Table 2), predicted-observed plots (Fig. 4) and normal probability plots of residuals (Fig. S7); (3) The significance of each variable was validated by exploiting ANOVA (Table 2), and the optimized polynomial models (Eqs. (4)–(7)) were subsequently obtained by removing statistically insignificant variables.

Generally, CCD-RSM is characterized by three operations including a full factorial design (2^k), a star design (axial points $2k$) and replicates at center points C_0 , where k denotes number of factors (Domínguez et al., 2010; Basiri Parsa et al., 2013; Nezhadali and Mojarrab, 2016). The three-factor CCD-RSM in this research is designed, which has been adopted in many previous design procedures (Velegraki et al., 2010; Basiri Parsa et al., 2013; Wang et al., 2020). Equations (S4) and (S5) (in Supplementary Text S4) are used for calculating axial low and high levels of R , v and i values. The various levels of the variables investigated are calculated as shown in Table S3. Figs. S3 and S4 show the fluctuating variations of effluent pollutant and ACS levels (Fig. S3) and pH, water temperature and conductivity levels and voltages (Fig. S4) in the

Table 2

ANOVA results of the polynomial models of COD removal (C_R , %), energy efficiency (C_E , g COD (kW h)⁻¹), effluent ACS level (C_A , mg L⁻¹) and toxic byproduct level (C_B , mg L⁻¹) in the CCD-RSM.

Source	Sum of Squares	df	Mean square	F-value	P-value
C_R (%)					
Model ^a	5432	3	1811	17	<0.0001*
R	322	1	322	3.0	0.10*
v	2051	1	2051	19	0.0005*
i	3058	1	3058	28	<0.0001*
Residuals	1749	16	109		
C_E (g COD (kW h)⁻¹)					
Model ^b	840	3	280	25	<0.0001*
R	42	1	42	3.8	0.07*
v	325	1	325	30	<0.0001*
i	473	1	473	43	<0.0001*
Residuals	176	16	11		
C_A (mg L⁻¹)					
Model ^c	88156	9	9795	93	<0.0001*
R	20657	1	20657	196	<0.0001*
v	17321	1	17320	164	<0.0001*
i	41565	1	41565	394	<0.0001*
R_V	325	1	325	3.1	0.10*
Ri	1596	1	1596	15	0.003*
vi	136	1	136	1.3	0.28
R^2	4088	1	4088	39	<0.0001*
v^2	1329	1	1329	13	0.01*
i^2	735	1	735	7.0	0.02*
Residuals	1056	10	106		
C_B (mg L⁻¹)					
Model ^d	0.60	3	0.20	12	0.0002*
R	0.07	1	0.07	4.2	0.06*
v	0.50	1	0.50	31	<0.0001*
i	0.03	1	0.03	2.0	0.17
Residuals	0.26	16	0.02		

*Statistically significant at $\alpha = 0.05$.

^a $R^2 = 0.76$; $R_{adj}^2 = 0.71$; adequate precision = 14.

^b $R^2 = 0.82$; $R_{adj}^2 = 0.79$; adequate precision = 17.

^c $R^2 = 0.99$; $R_{adj}^2 = 0.98$; adequate precision = 36.

^d $R^2 = 0.69$; $R_{adj}^2 = 0.64$; adequate precision = 11.

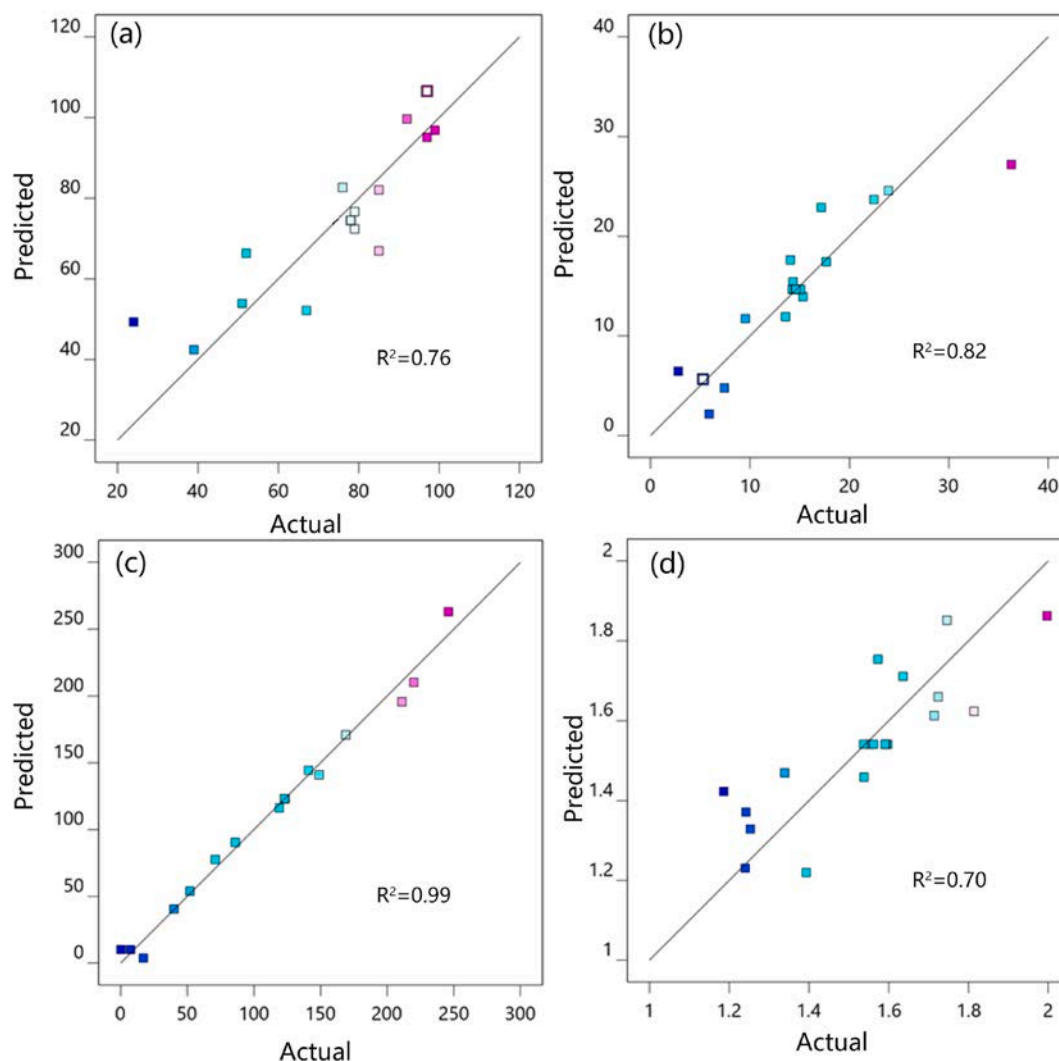


Fig. 4. Predicted versus actual values in the CCD-RSM: (a) COD removal, (b) energy efficiency, (c) effluent ACS level and (d) toxic byproduct level.

CCD-RSM experiments. On one hand ACS can effectively oxidize many pollutants, while on the other hand the formation of toxic organic byproducts (e.g., THMs and HAAs, constituting approximately 25% of total halogenated byproducts (Richardson et al., 2007)) could cause cytotoxicity and genotoxicity (Li et al., 2022). Fig. S5 shows the effluent levels of toxic byproducts in the CCD-RSM experiments. Dichloroacetic acid (DCAA) and trichloroacetic acid (TCAA) were the predominant toxic organic byproduct types, as observed in previous studies for treatment of industrial (Li et al., 2022) or municipal ROC (Bagastyo et al., 2012). Table S4 shows the CCD-RSM matrix and experimental values of responses corresponding to COD removal (C_R , %), energy efficiency (C_E , g COD (kW h)⁻¹), NH_4^+-N removal ($C_{R-\text{NH}_4^+-\text{N}}$, %), effluent ACS level (C_A , mg L⁻¹) and toxic byproduct level (C_B , mg L⁻¹). The COD removal was the major indicator for evaluating the performance of the CFS-C system, thus the NH_4^+-N removal model was not proposed. The regression models of C_R , C_E , C_A , and C_B are found as shown in Eqs. (S13)–(S16) (Supplementary Text S4). For the models of COD removal, energy efficiency and toxic byproduct level, no interaction and quadratic terms were detected, hence these models can be described adequately by simpler linear models. Specifically, the predictive accuracy of COD removal CCD-RSM model need to be further compared with previous PBD linear model. The interaction and quadratic terms were significant for the ACS level model, indicating that it was a quadratic nonlinear model.

Validation of the statistical results is analyzed using ANOVA pre-

sented in Table 2. Figs. 4 and S7 display the predicted-observed plots (Fig. 4) and normal probability plots of studentized residuals (Fig. S7). The E_{crit} value obtained was 3.62 for the models of COD removal, energy efficiency and toxic byproduct level, while that was 4.15 for the model of ACS level. The responses were well fitted to the models with high R^2 , R_{adj}^2 and adequate precision (Table 2). The model F and P values showed that the models estimated were significant at the 95% confidence level. Additionally, the excellent linear fits between predicted and observed values (Fig. 4), as well as normal distribution of calculated residuals (Fig. S7), indicated that all models were perspective in investigating the effects of influencing factors and that the residuals may be explained as random noises. To improve the predictive accuracy, the terms with P values less than 0.1 were still included in the CCD-RSM model. The ANOVA analysis of COD removal and energy efficiency showed that ν and i were highly significant model terms (i.e., $P < 0.05$) while R was significant terms (i.e., $P < 0.1$). From ANOVA for ACS level showed that R , ν , i , Ri , R^2 , ν^2 and i^2 were highly significant model terms while $R\nu$ was significant term. From ANOVA for toxic byproduct level showed that R was highly significant model terms while ν was significant term. The optimized polynomial equations for COD removal ($C_{R-COD(opt.)}$), energy efficiency ($C_{E(opt.)}$), effluent ACS level ($C_{A(opt.)}$) and toxic byproduct level ($C_{B(opt.)}$) are given below:

$$C_{R(opt.)} = 57.06 + 2.78R - 10.21\nu + 5.99i \quad (4)$$

$$C_{E(opt.)} = 14.61 + 1.0R + 4.07v - 2.35i \quad (5)$$

$$C_{A(opt.)} = -37.58 + 47.49R - 44.26v + 27.45i - 3.04Rv + 3.23Ri - 5.50R^2 + 6.67v^2 - 1.14i^2 \quad (6)$$

$$C_{B(opt.)} = 1.68 + 0.04R - 0.16v \quad (7)$$

Fig. S8 shows the comparison of experimental values of COD removal and effluent ACS level with CCD-RSM and PBD model predicted values. As for the COD removal, the discrepancy between experimental and predicted values became expectedly insignificant, implying that the CCD-RSM and PBD models were both adequate for predictions inside the range of conditions. However, the experimental data of effluent ACS level was more fitted to the CCD-RSM model than the PBD model, thus the CCD-RSM model was strongly recommended for parameter design of the CFS-C system.

3.3. Optimization of electrolytic parameters based on the CCD-RSM models

Contour diagrams and optimum conditions for different responses. To determine the optimum values of factors for COD removal, energy efficiency, effluent ACS and toxic byproduct levels, two-dimensional contour plots are constructed; these plots are shown in Fig. 5. As shown in Fig. 5a, the highest COD removal (>90%) can be achieved when R was higher than 5 and v was lower than 1.2 cm h^{-1} . In Fig. 5b, the highest COD removal can be achieved when i was higher than 7 mA cm^{-2} and R was higher than 3.6. In Fig. 5c, the highest COD removal can be achieved when i was higher than 6 mA cm^{-2} and v was lower than 2.4 cm h^{-1} . The slope of contour was primarily due to the variation of i and v , while R affected the slope slightly. The increase in R value from 1.5 to 5 resulted in a slight increase in the COD removal, probably due to a higher R value led to higher generation of ACS and thus the COD removal. The substantial effects of v value on the COD removal, reaction rate and energy consumption of the electrolytic process have been the objects of previous research (Dominguez-Ramos and Irbien, 2013). The decrease of v led to an increase in the COD removal, previous studies have also observed that decreasing the ratio of inlet flow to anode area (Dominguez-Ramos and Irbien, 2013) or inlet flow (Basha et al., 2012) can lead to a higher conversion of COD. This is because lower feed rates would increase the reactant: pollutant molar ratio and thus result in a higher probability of collision between the reactant species and pollutant compounds (Chanworrawoot and Hunsom, 2012). As for current density, it has been generally verified that higher current densities generally promoted ACS generation at the electrode surface, resulting in the rapid removal of organic pollutants (Li et al., 2022).

Previous researchers have evaluated the energy consumption of the two-stage electrochemical system enhanced by ultraviolet radiation (Ren et al., 2021) and sequential batch three-dimensional electrode reactor (Ren et al., 2023), aiming to assess the application potential of the electrolytic systems. To evaluate the application potential of CFS-C system, we calculated the energy efficiency (i.e., the amount of COD removed from ROC (in g COD) with the consumption of 1 kWh electrochemical energy), which has been used in our previous study (Li et al., 2022). As shown in Fig. 5d, the highest energy efficiency (>20 g COD (kW h)⁻¹) can be achieved when R was higher than 5 and v was higher than 3.6 cm h^{-1} . In Fig. 5e, the highest energy efficiency can be achieved when i was lower than 4 mA cm^{-2} and R was higher than 2.9. In Fig. 5f, the highest energy efficiency can be achieved when i was lower than 5 mA cm^{-2} and v was higher than 2.4 cm h^{-1} . The slope of contour was primarily due to the variation of i and v . The variation in the response due to the variation in R value was negligible, but the increase in R value resulted in a significant increase of energy consumption of recirculation pump. The increase in v value resulted in a significant increase in energy efficiency, as observed in previous studies (Basha et al., 2012; Li et al., 2013; Cho et al., 2020). This is because the introduction

of effluent recirculation enhanced the reutilization of long-lived oxidants in the buffer tank to enhance pollutant removal, thus resulting in the energy saving. Higher current densities generally result in a marked loss of electrical energy in the form of unwanted reactions (Li et al., 2022); this explains why a low energy efficiency of the CFS-C system was observed at a higher current density. Therefore, the simultaneous increase of R value and decrease of current density and v value could be an effective strategy to reduce the energy consumption of CFS-C system.

As shown in Fig. 5g, the lowest ACS level (<50 mg L⁻¹) can be achieved when R was lower than 3.6 and v was higher than 3.6 cm h^{-1} . In Fig. 5h, the lowest ACS level can be achieved when i was lower than 4 mA cm^{-2} and R was lower than 2.2. In Fig. 5i, the lowest ACS level can be achieved when i was lower than 3 mA cm^{-2} and v was higher than 3.0 cm h^{-1} . The interaction of R and i and the quadratic term of v^2 had positive effects on the response. The slope of contour was primarily due to the variation of v , while R and i affected the slope slightly. Significant amounts of ACS oxidants could be accumulated in the front buffer tank at a high R level and current density. In contrast, an extremely high level of v value had a negative effect on the accumulation of ACS oxidants.

As shown in Fig. 5j, the lowest toxic byproduct level (<1.3 mg L⁻¹) can be achieved when R was lower than 1.5 and v was higher than 3.6 cm h^{-1} . In Fig. 5k, the lowest toxic byproduct level (<1.45 mg L⁻¹) can be achieved when i was lower than 4 mA cm^{-2} and R was lower than 2.2. In Fig. 5l, the lowest toxic byproduct level (<1.4 mg L⁻¹) can be achieved when i was lower than 8 mA cm^{-2} and v was higher than 3.0 cm h^{-1} . The slope of contour was primarily due to the variation of v , while R and i affected the slope slightly. An increase in v value resulted in a marked decrease in effluent toxic byproduct level, i.e., reducing the total HRT was helpful to control the effluent toxic byproduct level. This is because the decrease of total HRT resulted in a decrease of collision probability between ACS oxidants and pollutants. Many factors have been reported to affect the effluent toxic byproduct levels, including cathode structure (Mao et al., 2012), cathode potential (Radjenović et al., 2012), current density (Mao et al., 2012; Zhao et al., 2014), HRT (Mao et al., 2012), and electrolyte level (Mao et al., 2012). Several methods have been devoted to the optimization for controlling the effluent toxic byproduct levels, including using high-performance electrodes and electrolysis cells, optimizing the operational conditions, and applying in combination with other remediation methods (Mao et al., 2012). In our previous study, the effluent total THMs and HAAs levels of the optimized CFS-C system are 0.17 and 2.1 mg L⁻¹, respectively (Li et al., 2022); these are still 2.1–5.2 and 25–47 fold respectively greater than the limit values of chlorinated drinking water (i.e., 80 and 60 µg L⁻¹ (Panizza and Cerisola, 2009)). In this study, the multivariate optimization was used to resolve the aforementioned problem, exploring the strategies to control the effluent toxic byproduct level, such as reducing the recirculation ratio, increasing the inflow linear velocity and reducing the current density.

The highest pollutant removal was achieved at a high R value, a high current density and a low v value; the highest energy efficiency was achieved at a high R , a low current density and a high v value; the lowest effluent ACS and toxic byproduct levels were achieved at a low R value, a low current density and a high v value. Therefore, in order to simultaneously achieve the maximum COD removal and energy efficiency and minimum effluent ACS and toxic byproduct levels, the multivariate optimization should be carried out for industrial ROC electrolytic treatment.

Multivariate optimization for industrial ROC electrolytic treatment. The simultaneous optimization of variables was performed using the multivariate optimization tool with desirability function as mentioned in previous studies (Kaur et al., 2018a, 2018b). Depending on the preferred targets (smaller-the-best: STB and larger-the-best: LTB) of the responses, the individual desirability transformation function is varied. In this study, the targets for the responses C_R and C_E were set as LTB, while C_A and C_B as STB. One-sided desirability d_i is used in the study given by (Mondal et al., 2013; Kaur et al., 2018b):

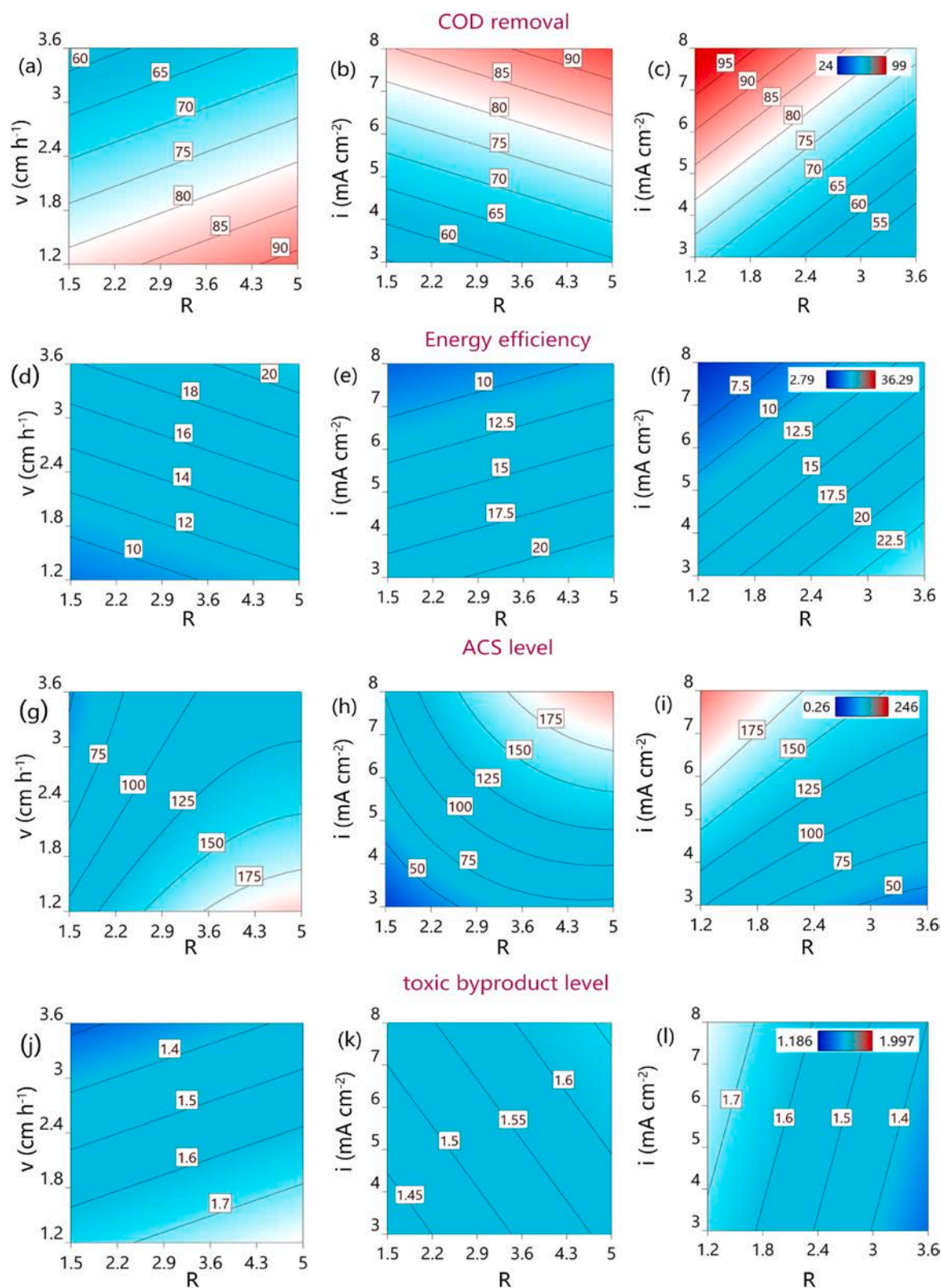


Fig. 5. Response contour diagrams of CCD-RSM design for the interactive effect of each pair of recirculation ratio (R), inflow linear velocity (v), and current density (i) on the COD removal, energy efficiency, effluent ACS and toxic byproduct levels where the other uninvolved factors are held at their respective center levels (i.e., recirculation ratio = 5.5, inflow linear velocity = 2.4 cm h⁻¹, current density = 5.5 mA/cm²). The change of color from blue to red means the increasing of the responses (i.e., from 24 to 99% for COD removal; from 2.79 to 36.29 g COD (kWh)⁻¹ for energy efficiency; from 0.26 to 246 mg L⁻¹ for ACS level; from 1.186 to 1.997 mg L⁻¹ for toxic byproduct level). (a, d, g, j): Responses for recirculation ratio vs. inflow linear velocity, (b, e, h, k): Responses for recirculation ratio vs. current density, (c, f, i, l): Responses for inflow linear velocity vs. current density.

$$d_i = \begin{cases} 0 & \text{if } C_i \leq C_{i-\min} \\ \left[\frac{C_i - C_{i-\min}}{C_{i-\max} - C_{i-\min}} \right]^r & \text{if } C_{i-\min} \leq C_i \leq C_{i-\max} \\ 1 & \text{if } C_i \geq C_{i-\max} \end{cases} \quad (8)$$

where, C_i is the response value, $C_{i-\min}$ or $C_{i-\max}$ is the minimum or maximum value of response i , and r is weight and a positive constant. This study set the weight of individual response according to its importance (Supplementary Text S5). The desirability for response C_R , C_E , C_A and C_B is calculated as shown in Eqs. (S17)–(S20) in Supplementary Text S5. The multivariate optimization is composed of a set of constraints as shown in Table S5.

We proposed a solution for the simultaneous optimization of R , v and i to guarantee effluent quality with less energy consumption (calculated as shown in Eq. (S21) in Supplementary Text S5). The most appropriate optimization conditions were found to be $R = 1$, $v = 3.3 \text{ cm h}^{-1}$, $i = 8 \text{ mA cm}^{-2}$ ($d = 2 \text{ cm}$ and $R_V = 20$), which showed the highest overall desirability, $d_4 = 0.57$. At these optimum conditions, the C_R , C_E , C_A and C_B were 74%, 10.2 g COD (kWh) $^{-1}$, 57 mg L $^{-1}$ and 1.36 mg L $^{-1}$, respectively. Therefore, it is impossible to find the optimum parameters those can simultaneously satisfy the ideal COD removal and energy efficiency as well as low effluent ACS and toxic byproduct levels. The simultaneous optimization of R and i was thus carried out to guarantee COD removal with less effluent ACS and toxic byproduct levels (calculated as shown in Eq. (S22) in Supplementary Text S5). The most appropriate optimization conditions were found to be $R = 1.0$, $i = 8 \text{ mA cm}^{-2}$ ($d = 2 \text{ cm}$, $R_V = 20$ and $v = 1.2 \text{ cm h}^{-1}$), which showed highest overall desirability, $d_3 = 0.72$. At these optimum conditions, the C_R , C_E , C_A and C_B were 95%, 1.7 g COD (kWh) $^{-1}$, 116 mg L $^{-1}$ and 1.69 mg L $^{-1}$, respectively. Following the multivariate optimization, the levels of effluent toxic byproducts (THMs and HAAs) were higher than the limit values of chlorinated drinking water (i.e., 140 $\mu\text{g L}^{-1}$ for THMs and 60 $\mu\text{g L}^{-1}$ for HAAs (Richardson et al., 2007)). Fig. 5l indicated that effluent toxic byproduct level increased obviously along with v , but had insignificant correlation with i . Therefore, the simultaneous increase of inflow load and current density can not only achieve the ideal COD removal, but also control the effluent toxic byproduct level. In future engineering practices, a high inflow load of CFS-C system should be set according to the COD removal CCD-RSM model.

4. Conclusions

The PBD and CCD-RSM models were efficient in analyzing the relations between variables and the responses. R , v values and current density significantly influenced COD and $\text{NH}_4^+ - \text{N}$ removal and effluent ACS level. High chloride content of industrial ROC facilitated the generation of ACS oxidants and subsequent mass transfer, and low HRT of CFS-C system improved the mass transfer efficiency. Moreover, the HRT of buffer tank in the CFS-C system was far higher than that of other advanced oxidation devices. Therefore, the electrode spacing and R_V value had negligible effects on the treatment performance of the CFS-C system. The critical values of R_V and electrode spacing should be further optimized to produce high quality of effluent with less fixed investment inputs. The process parameters can be adjusted to effectively control the performance of the CFS-C system according to the CCD-RSM models. The high R value, high current density and low v value facilitated COD removal, the high R value, low current density and high v value improved the energy efficiency, and the low R value, low current density and high v value reduced the effluent ACS and toxic byproduct levels. The most appropriate optimization conditions were found to be $v = 1.2 \text{ cm h}^{-1}$, $i \geq 8 \text{ mA cm}^{-2}$ (or calculated according to COD removal CCD-RSM polynomial model), $d \geq 4 \text{ cm}$, $R_V = 10 - 20$ and $R = 1.0$. In future engineering practices, a high inflow load of CFS-C system should be set according to the COD removal CCD-RSM polynomial model in order to simultaneously achieve the ideal COD removal and low effluent

toxic byproduct level.

Declaration of competing interest

The authors declare that they have no known competing financial interests or personal relationships that could have appeared to influence the work reported in this paper.

Data availability

Data will be made available on request.

Acknowledgements

This study was supported by the National Natural Science Foundation of China (No. 22176015 and 51878050).

Appendix A. Supplementary data

Supplementary data to this article can be found online at <https://doi.org/10.1016/j.chemosphere.2023.139078>.

References

- Armas, M.A., Maria-Hormigos, R., Cantalapiedra, A., Gismara, M.J., Sevilla, M.T., Procopio, J.R., 2016. Multiparametric optimization of a new high-sensitive and disposable mercury (II) electrochemical sensor. *Anal. Chim. Acta* 904, 76–82.
- Bagastyo, A.Y., Batstone, D.J., Kristiana, I., Gernjak, W., Joll, C., Radjenovic, J., 2012. Electrochemical oxidation of reverse osmosis concentrate on boron-doped diamond anodes at circumneutral and acidic pH. *Water Res.* 46 (18), 4951–4959.
- Bagastyo, A.Y., Radjenovic, J., Mu, Y., Rozendal, R.A., Batstone, D.J., Rabaey, K., 2011. Electrochemical oxidation of reverse osmosis concentrate on mixed metal oxide (MMO) titanium coated electrodes. *Water Res.* 45 (16), 4951–4959.
- Basha, C.A., Sendhil, J., Selvakumar, K.V., Muniswaran, P.K.A., Lee, C.W., 2012. Electrochemical degradation of textile dyeing industry effluent in batch and flow reactor systems. *Desalination* 285, 188–197.
- Basiri Parsa, J., Merati, Z., Abbasi, M., 2013. Modeling and optimizing of electrochemical oxidation of C.I. Reactive Orange 7 on the Ti/Sb-SnO₂ as anode via response surface methodology. *J. Ind. Eng. Chem.* 19 (4), 1350–1355.
- Chanworrawoot, K., Hunsom, M., 2012. Treatment of wastewater from pulp and paper mill industry by electrochemical methods in membrane reactor. *J. Environ. Manag.* 113, 399–406.
- Chatzisyemon, E., Xekoukoulakis, N.P., Diamadopoulos, E., Katsaounis, A., Mantzavinos, D., 2009. Boron-doped diamond anodic treatment of olive mill wastewaters: statistical analysis, kinetic modeling and biodegradability. *Water Res.* 43 (16), 3999–4009.
- Cho, S., Kim, C., Hwang, I., 2020. Electrochemical degradation of ibuprofen using an activated-carbon-based continuous-flow three-dimensional electrode reactor (3DER). *Chemosphere* 259, 127382.
- Cruz-González, K., Torres-López, O., García-León, A., Guzmán-Mar, J.L., Reyes, L.H., Hernández-Ramírez, A., Peralta-Hernández, J.M., 2010. Determination of optimum operating parameters for Acid Yellow 36 decolorization by electro-Fenton process using BDD cathode. *Chem. Eng. J.* 160 (1), 199–206.
- Ding, E., Cao, C., Hu, H., Chen, Y., Lu, X., 2020. Application of central composite design to the optimization of fly ash-based geopolymers. *Construct. Build. Mater.* 230, 116960.
- Dominguez-Ramos, A., Irabien, A., 2013. Analysis and modeling of the continuous electro-oxidation process for organic matter removal in urban wastewater treatment. *Ind. Eng. Chem. Res.* 52 (22), 7534–7540.
- Dominguez, J.R., González, T., Palo, P., Sánchez-Martín, J., 2010. Anodic oxidation of ketoprofen on boron-doped diamond (BDD) electrodes. Role of operative parameters. *Chem. Eng. J.* 162 (3), 1012–1018.
- Ghanbari, M., Hadian, A.M., Nourbakhsh, A.A., MacKenzie, K.J.D., 2017. Modeling and optimization of compressive strength and bulk density of metakaolin-based geopolymer using central composite design: a numerical and experimental study. *Ceram. Int.* 43 (1), 324–335.
- Ghosh, P., Mukherji, S., 2018. Optimization of media composition for enhancing carbazole degradation by *Pseudomonas aeruginosa* RS1. *J. Environ. Chem. Eng.* 6 (2), 2881–2891.
- Ihm, S., Al-Najdi, O.Y., Hamed, O.A., Jun, G., Chung, H., 2016. Energy cost comparison between MSF, MED and SWRO: case studies for dual purpose plants. *Desalination* 397, 116–125.
- Jin, P., Chang, R., Liu, D., Zhao, K., Zhang, L., Ouyang, Y., 2014. Phenol degradation in an electrochemical system with TiO₂/activated carbon fiber as electrode. *J. Environ. Chem. Eng.* 2 (2), 1040–1047.
- Kaur, P., Kushwaha, J.P., Sangal, V.K., 2018a. Electrocatalytic oxidative treatment of real textile wastewater in continuous reactor: degradation pathway and disposability study. *J. Hazard Mater.* 346, 242–252.

- Kaur, P., Kushwaha, J.P., Sangal, V.K., 2018b. Transformation products and degradation pathway of textile industry wastewater pollutants in Electro-Fenton process. *Chemosphere* 207, 690–698.
- Kaur, R., Kushwaha, J.P., Singh, N., 2019. Electro-catalytic oxidation of ofloxacin antibiotic in continuous reactor: evaluation, transformation products and pathway. *J. Electrochem. Soc.* 166 (6), 250–261.
- Lan, M., Li, M., Liu, J., Quan, X., Li, Y., Li, B., 2018. Coal chemical reverse osmosis concentrate treatment by membrane-aerated biofilm reactor system. *Bioresour. Technol.* 270, 120–128.
- Le, G.T., Ta, N.T., Pham, T.Q., Dao, Y.H., 2019. Response surface analysis of Fenobucarb removal by electrochemically generated chlorine. *Water* 11 (899), 1–15.
- Lee, L.Y., Ng, H.Y., Ong, S.L., Hu, J.Y., Tao, G., Kekre, K., Viswanath, B., Lay, W., Seah, H., 2009. Ozone-biological activated carbon as a pretreatment process for reverse osmosis brine treatment and recovery. *Water Res.* 43 (16), 3948–3955.
- Li, S., Zheng, S., Zheng, X., Bi, D., Yang, X., Luo, X., 2022. Optimization of electrolytic system type for industrial reverse osmosis concentrate treatment to achieve effluent quality and energy savings. *Sep. Purif. Technol.* 295, 121343.
- Li, W., Zhang, M., Wang, H., Lian, J., Qiang, Z., 2021. Removal of recalcitrant organics in reverse osmosis concentrate from coal chemical industry by UV/H₂O₂ and UV/PDS: efficiency and kinetic modeling. *Chemosphere* 287, 131999.
- Li, X., Zhu, W., Wang, C., Zhang, L., Qian, Y., Xue, F., Wu, Y., 2013. The electrochemical oxidation of biologically treated citric acid wastewater in a continuous-flow three-dimensional electrode reactor (CTDER). *Chem. Eng. J.* 232, 495–502.
- Liu, L., Cai, W.F., Chen, Y.Q., Wang, Y., 2018. Fluid dynamics and mass transfer study of electrochemical oxidation by CFD prediction and experimental validation. *Ind. Eng. Chem. Res.* 57 (18), 6493–6504.
- Liu, X., Novak, J.T., He, Z., 2019a. Removal of landfill leachate ultraviolet quenching substances by electricity induced humic acid precipitation and electrooxidation in a membrane electrochemical reactor. *Sci. Total Environ.* 689, 571–579.
- Liu, Z.Q., You, L.H., Xiong, X.J., Wang, Q., Yan, Y.H., Tu, J.L., Cui, Y.H., Li, X.Y., Wen, G., Wu, X.H., 2019b. Potential of the integration of coagulation and ozonation. *Chemosphere* 222, 696–704.
- Mao, X., Ciblak, A., Baek, K., Amiri, M., Loch-Carusio, R., Alshawabkeh, A.N., 2012. Optimization of electrochemical dechlorination of trichloroethylene in reducing electrolytes. *Water Res.* 46 (6), 1847–1857.
- Martinez-Huitle, C.A., Rodrigo, M.A., Sires, I., Scialdone, O., 2015. Single and coupled electrochemical processes and reactors for the abatement of organic water pollutants: a critical review. *Chem. Rev.* 115 (24), 13362–13407.
- Mondal, B., Srivastava, V.C., Kushwaha, J.P., Bhatnagar, R., Singh, S., Mall, I.D., 2013. Parametric and multiple response optimization for the electrochemical treatment of textile printing dye-bath effluent. *Sep. Purif. Technol.* 109, 135–143.
- Ndlwana, L., Motsa, M.M., Mamba, B.B., 2020. A unique method for dopamine-cross-linked graphene nanoplatelets within polyethersulfone membranes (GNP-pDA/PES) for enhanced mechanochemical resistance during NF and RO desalination. *Eur. Polym. J.* 136, 109889.
- Nezhadali, A., Mojarab, M., 2016. Computational design and multivariate optimization of an electrochemical metoprolol sensor based on molecular imprinting in combination with carbon nanotubes. *Anal. Chim. Acta* 924, 86–98.
- Panagopoulos, A., Haralambous, K.J., Loizidou, M., 2019. Desalination brine disposal methods and treatment technologies-A review. *Sci. Total Environ.* 693, 133545.
- Panizza, M., Cerisola, G., 2009. Direct and mediated anodic oxidation of organic pollutants. *Chem. Rev.* 109, 6541–6569.
- Radjenovic, J., Bagastyo, A., Rozendal, R.A., Mu, Y., Keller, J., Rabaey, K., 2011. Electrochemical oxidation of trace organic contaminants in reverse osmosis concentrate using RuO₂/IrO₂-coated titanium anodes. *Water Res.* 45 (4), 1579–1586.
- Radjenović, J., Farre, M.J., Mu, Y., Gernjak, W., Keller, J., 2012. Reductive electrochemical remediation of emerging and regulated disinfection byproducts. *Water Res.* 46 (6), 1705–1714.
- Ren, X., Song, K., Chen, W., Liu, J., Liu, D., 2021. Treatment of membrane concentrated leachate by two-stage electrochemical process enhanced by ultraviolet radiation: performance and mechanism. *Sep. Purif. Technol.* 259, 118032.
- Ren, X., Tang, P., Hou, B., Yu, Z., Huang, J., Wang, Q., Song, K., 2023. Evaluating the degradation of Rhodamine B using a sequential batch three-dimensional electrode reactor. *J. Environ. Chem. Eng.* 11 (2), 109475.
- Richardson, S.D., Plewa, M.J., Wagner, E.D., Schoeny, R., Demarini, D.M., 2007. Occurrence, genotoxicity, and carcinogenicity of regulated and emerging disinfection by-products in drinking water: a review and roadmap for research. *Mutat. Res.* 636 (1–3), 178–242.
- Shi, J., Huang, W., Han, H., Xu, C., 2020. Review on treatment technology of salt wastewater in coal chemical industry of China. *Desalination* 493, 114640.
- Soriano, Á., Gorri, D., Urriaga, A., 2019. Membrane preconcentration as an efficient tool to reduce the energy consumption of perfluorohexanoic acid electrochemical treatment. *Sep. Purif. Technol.* 208, 160–168.
- Thakur, C., Srivastava, V.C., Mall, I.D., 2009. Electrochemical treatment of a distillery wastewater: parametric and residue disposal study. *Chem. Eng. J.* 148 (2–3), 496–505.
- Tijing, L.D., Woo, Y.C., Choi, J.S., Lee, S., Kim, S.H., Shon, H.K., 2015. Fouling and its control in membrane distillation-A review. *J. Membr. Sci.* 475, 215–244.
- Velegraki, T., Balayiannis, G., Diamadopoulos, E., Katsaounis, A., Mantzavinos, D., 2010. Electrochemical oxidation of benzoic acid in water over boron-doped diamond electrodes: statistical analysis of key operating parameters, kinetic modeling, reaction by-products and ecotoxicity. *Chem. Eng. J.* 160 (2), 538–548.
- Wang, J., Yao, J., Wang, L., Xue, Q., Hu, Z., Pan, B., 2020. Multivariate optimization of the pulse electrochemical oxidation for treating recalcitrant dye wastewater. *Sep. Purif. Technol.* 230, 115851.
- Zhang, C., Wang, J., Zhou, H., Fu, D., Gu, Z., 2010. Anodic treatment of acrylic fiber manufacturing wastewater with boron-doped diamond electrode: a statistical approach. *Chem. Eng. J.* 161 (1–2), 93–98.
- Zhao, X., Li, A.Z., Mao, R., Liu, H.J., Qu, J.H., 2014. Electrochemical removal of haloacetic acids in a three-dimensional electrochemical reactor with Pd-GAC particles as fixed filler and Pd-modified carbon paper as cathode. *Water Res.* 51, 134–143.